JOURNAL OF MOLECULAR SPECTROSCOPY **138,** 251–263 (1989)

High-Resolution Spectroscopy on the $\tilde{A}\,^1B_1(0, 6, 0) \leftarrow \tilde{X}\,^1A_1(0, 0, 0)$ Transition in $SiCl_2$

GERARD MEIJER,[1] JOHANNES HEINZE, W. LEO MEERTS, AND J. J. TER MEULEN

Department of Molecular and Laser Physics, University of Nijmegen, Toernooiveld, 6525 ED Nijmegen, The Netherlands

AND

JON T. HOUGEN[2]

Molecular Spectroscopy Division, National Institute of Standards and Technology, Gaithersburg, Maryland 20899

High-resolution laser-induced fluorescence spectra of $Si^{35}Cl_2$ and $Si^{35}Cl^{37}Cl$ have been observed in a molecular beam. A spectral resolution of 8 MHz was obtained on the $\tilde{A}\,^1B_1(0, 6, 0) \leftarrow \tilde{X}\,^1A_1(0, 0, 0)$ transition around 323 nm, which allowed the dense rotational structure of this electronic transition to be completely resolved. The rotational constants in the $\tilde{A}\,^1B_1(0, 6, 0)$ state reflect the almost 22° opening of the ClSiCl bond angle on going from $\tilde{X}$ to $\tilde{A}$, whereas the Si–Cl bond length decreases slightly.

1. INTRODUCTION

The UV spectrum of the $SiCl_2$ radical has been subject to some confusion. Exactly fifty years ago Asundi *et al.* (*1*) reported a structured emission spectrum in the 310–390 nm region, which they attributed to the $SiCl_2$ radical. In 1977 Cornet and Dubois (*2*) showed, however, that these emission bands belonged to well known electronic transitions of PO and P_2 radicals. Although in the meantime Wieland and Heise (*3*) mentioned having observed a continuous absorption spectrum of $SiCl_2$ produced in a reaction of Si with $SiCl_4$, the first reliable absorption spectrum of $SiCl_2$ was recorded by Milligan and Jacox (*4*). They observed a broad ($\approx$5 nm halfwidth) unstructured absorption around 315 nm while studying the IR spectrum of Ar matrix isolated $SiCl_2$ produced by photolysis of Ar:SiH_2Cl_2 and Ar:SiD_2Cl_2 samples at liquid helium temperatures. About three years ago the first $SiCl_2$ ($\tilde{A}\,^1B_1 \leftarrow \tilde{X}\,^1A_1$) absorption bands in the gas phase were reported by Ruzsicska *et al.* (*5*). In the flash photolysis of Si_2Cl_6 they observed a broad absorption band showing a partly resolved ν_2' progression. From this time on the unraveling of the electronic spectrum of $SiCl_2$ proceeded rapidly. Washida *et al.* (*6*) observed a broad emission spectrum following the photolysis of SiH_2Cl_2 and $SiHCl_3$. A similar emission spectrum, but now with partly resolved vi-

[1] Present address: IBM, Almaden Research Center, 650 Harry Road, San José, California 95120-6099.

[2] Nederlandse Organisatie voor Wetenschappelijk Onderzoek, visiting scientist University of Nijmegen, Spring 1988.

0022-2852/89 $3.00

brational structure, was observed in the flash photolysis of methylchlorosilanes by Sameith *et al.* (*7*). They found good agreement with the absorption data (*5*) and the partly resolved isotope shift allowed them a first assignment of the vibrational transitions. More recently Suzuki *et al.* (*8*) were the first to apply the LIF technique to the $SiCl_2$ radical. Using a pulsed laser they measured both laser excitation spectra and dispersed fluorescence spectra of the $SiCl_2$ $\tilde{A}^1B_1 \leftarrow \tilde{X}^1A_1$ transition. From these spectra they reassigned the vibrational bands, and in addition determined several new vibrational transitions. Although the rotational structure in the vibrational bands was not resolved, accurate positions for the band origins were given. The collision-free radiative lifetime of the $\tilde{A}^1B_1$ ($\nu_2' = 7$) state was measured to be (77 ± 3) ns. This value is much more directly determined, and therefore much more reliable, than the lifetime of 4.5 μs reported previously in the IR multiphoton dissociation of SiH_2Cl_2 (*9*).

Microwave spectra of the $SiCl_2$ radical were recently observed by Tanimoto *et al.* (*10*). They determined the molecular constants for the $\tilde{X}^1A_1(0, 0, 0)$ states of both the $Si^{35}Cl_2$ and the $Si^{35}Cl^{37}Cl$ isotopic species by least-squares fits to 22 and 17, respectively, observed microwave transitions. The rotational constants they found confirm the results of recent ab initio calculations by Gosavi and Strausz (*11*) and by Ha *et al.* (*12*).

Here we present the first rotationally resolved vibrational band of the $SiCl_2$ $\tilde{A}^1B_1 \leftarrow \tilde{X}^1A_1$ transition. Using a cw intracavity frequency doubled ring dye laser in connection with a molecular beam machine high resolution LIF spectra were recorded. The width of the spectral lines was typically 30 MHz. To get an even higher resolution a pump-probe technique was applied in some dense regions of the spectrum, yielding linewidths down to 8 MHz. The observed spectra are analyzed using the known ground state constants (*10*). For both $Si^{35}Cl_2$ and $Si^{35}Cl^{37}Cl$ the rotational structure in the $\tilde{A}^1B_1(0, 6, 0)$ state is determined. For the vibrational band under study the band origin as well as the isotope shift are determined very accurately.

2. EXPERIMENTAL DETAILS

The $SiCl_2$ radicals are produced in a microwave discharge (100 W at 2.45 GHz) in a flowing gas mixture of $SiHCl_3$ diluted in Ar. The coaxial microwave discharge cavity we used, has been described previously (*13*). For the analysis of the $SiCl_2$ spectrum it is a disadvantage that the radicals are normally formed rotationally and vibrationally hot in our source; in the high-resolution study of SiCl, produced in a similar discharge of $SiCl_4$ in Ar, a rotational temperature of about 800 K is deduced from the LIF spectrum (*14*). The $SiCl_2$ radicals, however, turned out to be quite stable, which makes a certain cooling due to wall collisions possible. Therefore, we pulled back our microwave cavity a little, which implies that the produced radicals have to travel over a length of about 5 cm through the 9-mm inner diameter quartz tube, at a pressure around 1 mbar. Although the rotational temperature of the $SiCl_2$ radicals is still estimated to be 400 K (from the LIF spectrum), a considerable simplification of the LIF spectrum is obtained. Furthermore the fluorescence background from the discharge region is largely reduced. A similar method has been used to simplify the electronic spectrum of the unstable SiF_2 molecule (*15*). After several hours of operation the first 5 cm of the quartz tube were clogged completely with polymeric $(SiCl_2)_n$. Clogging

of the beam orifice, which is a 2.5-mm diameter circular hole in a brass plate, could be avoided by heating this up to $\approx$500 K.

The molecular beam machine, the UV production, and the LIF detection zone have been described previously (*13, 16*), and only a brief summary is given here. The $SiCl_2$ radicals are detected by LIF, in a region about 15 cm downstream from the beam orifice, where the unfocused UV laser beam crosses the molecular beam perpendicularly. With about 5 mW of tunable UV radiation around 323 nm the $SiCl_2$ $\tilde{X}^1A_1(0, 0, 0)$ radicals are excited to the $\tilde{A}^1B_1(0, 6, 0)$ state. Total laser-induced fluorescence from single populated rotational levels in this excited state to the different vibrational levels in the electronic ground state (*8*) is detected. To shield for the fluorescence background from the discharge region a set of filters transmitting essentially in the 320–350 nm region are inserted in front of the PMT.

The observed spectral linewidth of about 30 MHz is determined mainly by the residual Doppler broadening due to the divergence of the molecular beam. In order to reach a higher spectral resolution we used a Doppler-free pump-probe technique in the molecular beam, details of which are given elsewhere (*17*). Now two counter-propagating laser beams are used, crossing the molecular beam in well-separated regions ($\approx$6 cm apart). The hole burned in the ground state population by the first laser is detected as a Lamb dip in the total fluorescence signal induced by the probe laser. As the Lamb dip signal is quadratically dependent on the applied cw laser power, higher UV laser powers (between 10–15 mW) were used. With a laser power of 15 mW through a 1-mm^2 area we could deplete about 30% of the ground state population for a given J''-level (on a Q line).

The UV radiation is obtained by frequency doubling in a $LiIO_3$ crystal inside the cavity of a single-frequency ring-dye laser operating on DCM dye. A UV power of 3–5 mW (0.5 MHz bandwidth) is obtained by pumping with 5 W of an Ar-ion laser (all lines). A somewhat higher pump power of 7 W is needed to produce the 10–15 mW tunable UV laser power used in the Lamb dip experiment.

The $SiCl_2$ spectra were recorded together with the transmission peaks of two temperature- and pressure-stabilized interferometers with a free spectral range (in the UV) of (598.82 $\pm$ 0.04) MHz and (148.25 $\pm$ 0.05) MHz, respectively. Several partly overlapping laser scans were made over a total region of $\approx$10 cm^{-1}. The positions of the $SiCl_2$ lines were measured in terms of the FSR of the interferometers. The absolute frequency of the transmission peaks of the interferometers, and thereby the absolute frequency of the $SiCl_2$ lines, was determined by the simultaneous recording of the I_2 absorption spectrum in a cell at the fundamental laser frequency. The correction to the wavelengths in the I_2-atlas of -0.0056 cm^{-1} was taken into account (*18*). By averaging over the 20 strongest and best determined I_2-lines in the scanned region, an accuracy of about 100 MHz could be obtained for the absolute frequency. This error is due to both the drift of the interferometers and the inaccuracy in the determination of the center of the broad and not always symmetric I_2-lines. Relative line positions were measured to an accuracy of 15 MHz.

3. ROTATIONAL ANALYSIS

In Fig. 1 a simplified schematic representation of a vibrational band in the $SiCl_2$ $\tilde{A} \leftarrow \tilde{X}$ electronic transition is shown. The $SiCl_2$ radical is a slightly asymmetric prolate

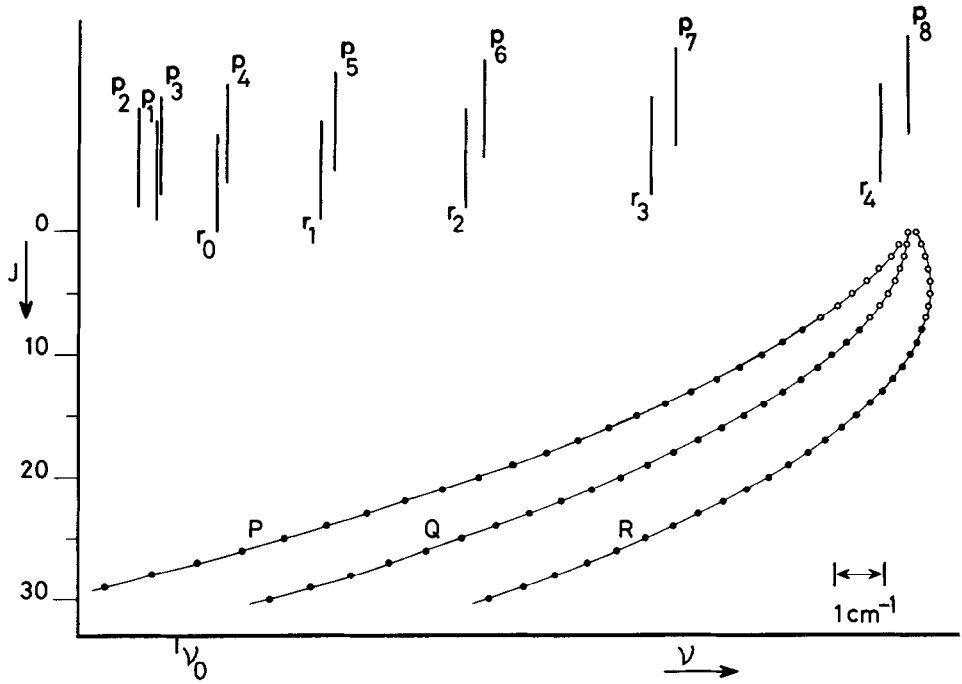

FIG. 1. Schematic representation of a vibrational band in the $Si^{35}Cl_2$ $\tilde{A} \leftarrow \tilde{X}$ transition, using the symmetric top approximation. The vertical bars in the upper part of the figure indicate the position of the different ΔK sub-band origins.

top with values for the asymmetry parameter (*19*) $\kappa = -0.927$ for $\tilde{X}\,^1A_1(0, 0, 0)$ (*10*) and $\kappa = -0.982$ for $\tilde{A}\,^1B_1(0, 6, 0)$. Nevertheless, Fig. 1 is drawn using the purely prolate symmetric top formulae for both the $\tilde{X}$ and the $\tilde{A}$ state. The horizontal scale is a frequency scale (cm^{-1}), and the position of the vibrational band origin is indicated by ν_0. The vertical bars in the upper part of the figure indicate the position of the calculated origins of the ΔK sub-bands; the $SiCl_2$ $\tilde{A} \leftarrow \tilde{X}$ transition is a perpendicular transition and both possible ΔK branches are given. Due to the relatively large opening in ClSiCl bond angle on going from $\tilde{X}$ to $\tilde{A}$, the change in the rotational constant A is very large. This is the reason for the bandhead in the P branch ($\Delta K = -1$) at such a low value of K_a''. Although this makes the spectral structure for $\nu > \nu_0$ more complex, it has the advantage that both P and R branches can be measured in the same spectral region, which increases the accuracy considerably.

Each ΔK sub-band has its own $\Delta J = 0, \pm 1$ branches, starting from the lowest rotational $J = K$ level. Only for the p_8 sub-band the three rotational branches are shown. The black dots represent the possible lines for this sub-band. The J-numbering for the P, Q, and R branches is indicated along the vertical axis in the figure. As $\bar{B}' < \bar{B}''$ ($\bar{B}$ is the average of the B and C rotational constants) these branches are red-degraded.

It is needless to say that for low values of K_a and/or high values of J the symmetric top approximation is no longer correct. The K-type doubling due to the asymmetric rotor behavior, especially in the $\tilde{X}\,^1A_1(0, 0, 0)$ ground state, can then no longer be ignored.

It is seen in Fig. 1 that the separation between consecutive lines of a rotational branch is large and increases quickly with increasing J''. For those J'' levels that are maximally populated in our beam ($J'' = 25$–50) successive lines of a branch are typically 1 cm^{-1} apart. With a typical spectral linewidth of 0.001 cm^{-1} in our set-up, needed to resolve single rotational lines, this means rotational branches cannot easily be recognized as such. The spectrum is further complicated by the presence of the $Si^{35}Cl^{37}Cl$ isotope, which is only a factor of $\frac{3}{2}$ less abundant. For both isotopes there is also the $\tilde{A}^1B_1(0, 5, 0) \leftarrow \tilde{X}^1A_1(0, 0, 0)$ band, with rotational lines in the same spectral region, which are expected to be reasonably strong. In addition hot bands will be present.

We started the experiment by making several overlapping scans and recording the $SiCl_2$ $\tilde{A} \leftarrow \tilde{X}$ spectrum in the 30 928.4–30 938.0 cm^{-1} region, about 30 cm^{-1} up from the expected $Si^{35}Cl_2$ $\tilde{A}^1B_1(0, 6, 0) \leftarrow \tilde{X}^1A_1(0, 0, 0)$ band origin (*8*). As seen from Fig. 1 only high K''_a-levels ($K''_a \geq 5$) are expected to be seen in this region. The corresponding band origin of the $Si^{35}Cl^{37}Cl$ isotope is known to be shifted to lower frequencies by 8–9 cm^{-1} (*8*), so even higher values of K''_a are expected for this isotope. The branch-finding procedure we used was based on the fact that the spectrum can be described here using the prolate symmetric top formulae. When centrifugal distortion corrections are neglected, it is easy to show that the rate at which the rotational lines in a branch walk out is then equal to $2\Delta\bar{B}$ for P, Q, and R branches. We just measured the exact position of about 300 strong lines (intensity $\geq$50% of the intensity of the strongest line), and let the computer search for branches using a constant walking-out rate as a criterion. Only sets of at least five successive lines were regarded as possible branches. In this way around 15 branches, each consisting of 5–19 lines, were found. Using the known rotational structure in the ground state (*10*) a consistent J, K labeling for the $Si^{35}Cl_2$ isotope as well as for the $Si^{35}Cl^{37}Cl$ isotope could be found by trial and error. In fact, a few of the computer-selected branches showed clearly the K-type doubling for higher J''. As the observed splittings are almost completely determined by the known (*10*) splittings in the $\tilde{X}^1A_1(0, 0, 0)$ state, these branches were the first to be unambiguously identified.

For $Si^{35}Cl_2$ and $Si^{35}Cl^{37}Cl$ total numbers of 315 and 189 resolved rotational transitions, respectively, were identified and included in a least squares fit to the asymmetric rotor model (*20*). The transitions are listed in Table I and Table II. In the first fits the ground state constants were kept fixed (*10*), which guaranteed the assignment to be correct. Lines of all six branches expected to be in the scanned region were included in the fit. For $Si^{35}Cl_2$ the ${}^rR$, ${}^rQ$, and ${}^rP$ branches for $K''_a = 5$–9 and the ${}^pR$, ${}^pQ$, and ${}^pP$ branches for $K''_a = 9$–14 were taken into account. In total, transitions to 194 different rotational levels in $\tilde{A}^1B_1(0, 6, 0)$ ($K'_a = 6$–13, with J' values up to 60) were fitted. For $Si^{35}Cl^{37}Cl$ $\tilde{A}^1B_1(0, 6, 0)$ the rotational structure for $K'_a = 7$–13, with J' values as high as $J' = 55$, was measured (transitions to 156 different rotational levels).

In the final fits microwave data (*10*) and optical data were fitted simultaneously. The experimental error in the microwave data (30 kHz (*10*)) is much smaller than the experimental error in the optical data (15 MHz), and therefore most ground state constants are mainly determined by the microwave data. However, especially the centrifugal distortion constants were much better determined by the higher J, K values of the optical data. All the ground state parameters obtained in fitting microwave data

TABLE I

Measured Transitions of the $Si^{35}Cl_2$ $\tilde{A}^1B_1(0, 6, 0) \leftarrow \tilde{X}^1A_1(0, 0, 0)$ Band (in Case of Unresolved K-Type Doubling the Second (K_1', K_1'') Combination Is Given in Parentheses)

J′	K_{-1}'	K_1'	J″	K_{-1}''	K_1''	wavenumber	error	J′	K_{-1}'	K_1'	J″	K_{-1}''	K_1''	wavenumber	error
10	6	4 (5)	11	5	6 (7)	30928.6831	0.0005	23	8	15 (16)	23	7	17 (16)	30937.7645	0.0005
6	6	0 (1)	5	5	0 (1)	30932.5936	0.0005	24	8	16 (17)	24	7	18 (17)	30937.0748	0.0005
7	6	1 (2)	6	5	1 (2)	30932.5694	0.0005	25	8	17 (18)	25	7	19 (18)	30936.3543	0.0005
8	6	2 (3)	7	5	2 (3)	30932.5173	0.0005	26	8	18 (19)	26	7	20 (19)	30935.6030	0.0005
9	6	3 (4)	8	5	3 (4)	30932.4357	0.0007	27	8	19 (20)	27	7	21 (20)	30934.8210	0.0005
10	6	4 (5)	9	5	4 (5)	30932.3264	0.0007	28	8	20 (21)	28	7	22 (21)	30934.0083	0.0005
11	6	5 (6)	10	5	5 (6)	30932.1877	0.0005	29	8	21 (22)	29	7	23 (22)	30933.1639	0.0010
12	6	6 (7)	11	5	6 (7)	30932.0204	0.0005	30	8	23	30	7	23	30932.2871	0.0005
13	6	7 (8)	12	5	7 (8)	30931.8237	0.0005	30	8	22	30	7	24	30932.2884	0.0005
14	6	8 (9)	13	5	8 (9)	30931.5976	0.0005	31	8	24	31	7	24	30931.3785	0.0005
15	6	9 (10)	14	5	9 (10)	30931.3422	0.0005	31	8	24	31	7	25	30931.3807	0.0005
16	6	10 (11)	15	5	10 (11)	30931.0568	0.0005	32	8	25	32	7	25	30930.4383	0.0005
17	6	11 (12)	16	5	11 (12)	30930.7417	0.0007	32	8	24	32	7	26	30930.4410	0.0005
18	6	12 (13)	17	5	12 (13)	30930.3952	0.0007	33	8	26	33	7	26	30929.4650	0.0005
19	6	13	18	5	13	30930.0176	0.0005	33	8	25	33	7	27	30929.4691	0.0005
19	6	14	18	5	14	30930.0192	0.0005	34	8	27	34	7	27	30928.4587	0.0005
20	6	14	19	5	14	30929.6100	0.0007	34	8	26	34	7	28	30928.4651	0.0005
20	6	15	19	5	15	30929.6128	0.0005	30	8	22 (23)	29	7	22 (23)	30937.5188	0.0005
21	6	15	20	5	15	30929.1703	0.0005	31	8	23	30	7	23	30936.7869	0.0005
15	7	8 (9)	16	6	10 (11)	30932.2918	0.0005	31	8	24	30	7	24	30936.7885	0.0005
16	7	9 (10)	17	6	11 (12)	30931.6606	0.0005	32	8	25	31	7	25	30936.0264	0.0005
17	7	10 (11)	18	6	12 (13)	30931.0003	0.0010	33	8	25	32	7	25	30935.2291	0.0005
20	7	13 (14)	21	6	15 (16)	30928.8371	0.0005	33	8	26	32	7	26	30935.2318	0.0005
8	7	1 (2)	8	6	3 (2)	30937.4494	0.0005	34	8	26	33	7	26	30934.4012	0.0005
9	7	2 (3)	9	6	4 (3)	30937.1957	0.0005	34	8	27	33	7	27	30934.4054	0.0005
10	7	3 (4)	10	6	5 (4)	30936.9135	0.0005	35	8	27	34	7	27	30933.5404	0.0005
11	7	4 (5)	11	6	6 (5)	30936.6028	0.0005	35	8	28	34	7	28	30933.5465	0.0005
12	7	5 (6)	12	6	7 (6)	30936.2633	0.0005	36	8	28	35	7	28	30932.6452	0.0007
13	7	6 (7)	13	6	8 (7)	30935.8947	0.0005	36	8	29	35	7	29	30932.6544	0.0005
14	7	7 (8)	14	6	9 (8)	30935.4967	0.0005	37	8	29	36	7	29	30931.7161	0.0005
15	7	8 (9)	15	6	10 (9)	30935.0702	0.0005	37	8	30	36	7	30	30931.7301	0.0005
16	7	9 (10)	16	6	11 (10)	30934.6138	0.0005	38	8	31	37	7	31	30930.7720	0.0005
17	7	10 (11)	17	6	12 (11)	30934.1286	0.0005	39	8	31	38	7	31	30929.7534	0.0005
18	7	11 (12)	18	6	13 (12)	30933.6130	0.0005	39	8	32	38	7	32	30929.7805	0.0005
19	7	12 (13)	19	6	14 (13)	30933.0676	0.0005	40	8	32	39	7	32	30928.7174	0.0010
20	7	13 (14)	20	6	15 (14)	30932.4917	0.0005	40	8	33	39	7	33	30928.7563	0.0005
21	7	14 (15)	21	6	16 (15)	30931.8856	0.0005	28	9	19 (20)	29	8	21 (22)	30936.9687	0.0005
22	7	15 (16)	22	6	17 (16)	30931.2490	0.0005	29	9	20 (21)	30	8	22 (23)	30935.9587	0.0005
23	7	16 (17)	23	6	18 (17)	30930.5813	0.0010	31	9	22 (23)	32	8	24 (25)	30933.8460	0.0010
24	7	18	24	6	18	30929.8816	0.0005	32	9	23 (24)	33	8	25 (26)	30932.7430	0.0005
24	7	17	24	6	19	30929.8832	0.0005	33	9	24 (25)	34	8	26 (27)	30931.6085	0.0005
25	7	19	25	6	19	30929.1508	0.0005	35	9	26 (27)	36	8	28 (29)	30929.2449	0.0010
25	7	18	25	6	20	30929.1533	0.0005	33	9	24 (25)	33	8	26 (25)	30937.5350	0.0005
14	7	7 (8)	13	6	7 (8)	30937.9261	0.0005	34	9	25 (26)	34	8	27 (26)	30936.5460	0.0005
15	7	8 (9)	14	6	8 (9)	30937.6737	0.0005	35	9	26 (27)	35	8	28 (27)	30935.5250	0.0005
16	7	9 (10)	15	6	9 (10)	30937.3920	0.0005	36	9	27 (28)	36	8	29 (28)	30934.4724	0.0005
17	7	10 (11)	16	6	10 (11)	30937.0813	0.0005	37	9	29	37	8	29	30933.3870	0.0005
18	7	11 (12)	17	6	11 (12)	30936.7410	0.0005	37	9	28	37	8	30	30933.3879	0.0005
19	7	12 (13)	18	6	12 (13)	30936.3703	0.0005	38	9	30	38	8	30	30932.2693	0.0005
20	7	13 (14)	19	6	13 (14)	30935.9701	0.0005	38	9	29	38	8	31	30932.2715	0.0005
21	7	14 (15)	20	6	14 (15)	30935.5396	0.0005	39	9	31	39	8	31	30931.1188	0.0005
22	7	15 (16)	21	6	15 (16)	30935.0789	0.0005	40	9	32	40	8	32	30929.9344	0.0005
23	7	16 (17)	22	6	16 (17)	30934.5873	0.0005	40	9	31	40	8	33	30929.9387	0.0005
24	7	17	23	6	17	30934.0645	0.0007	41	9	33	41	8	33	30928.7174	0.0010
24	7	18	23	6	18	30934.0654	0.0007	41	9	32	41	8	34	30928.7239	0.0005
25	7	18	24	6	18	30933.5111	0.0005	39	9	30 (31)	38	8	30 (31)	30937.9336	0.0005
25	7	19	24	6	19	30933.5124	0.0005	40	9	31	39	8	31	30936.9263	0.0005
26	7	19	25	6	19	30932.9255	0.0005	40	9	32	39	8	32	30936.9293	0.0005
26	7	20	25	6	20	30932.9277	0.0005	41	9	32	40	8	32	30935.8876	0.0005
27	7	20	26	6	20	30932.3075	0.0007	41	9	33	40	8	33	30935.8923	0.0005
27	7	21	26	6	21	30932.3111	0.0007	42	9	33	41	8	33	30934.8154	0.0005
28	7	21	27	6	21	30931.6575	0.0005	43	9	34	42	8	34	30933.7096	0.0010
28	7	22	27	6	22	30931.6630	0.0005	43	9	35	42	8	35	30933.7190	0.0005
29	7	22	28	6	22	30930.9745	0.0005	44	9	36	43	8	36	30932.5817	0.0005
29	7	23	28	6	23	30930.9836	0.0005	45	9	36	44	8	36	30931.3923	0.0005
30	7	23	29	6	23	30930.2579	0.0005	45	9	37	44	8	37	30931.4115	0.0010
30	7	24	29	6	24	30930.2707	0.0005	46	9	37	45	8	37	30930.1803	0.0005
31	7	24	30	6	24	30929.5070	0.0005	47	9	38	46	8	38	30928.9322	0.0005
31	7	25	30	6	25	30929.5260	0.0005	47	9	39	46	8	39	30928.9683	0.0005
18	8	10 (11)	19	7	12 (13)	30937.4664	0.0005	8	8	0 (1)	9	9	0 (1)	30930.0350	0.0005
19	8	11 (12)	20	7	13 (14)	30936.7508	0.0005	9	8	1 (2)	10	9	1 (2)	30929.6092	0.0007
20	8	12 (13)	21	7	14 (15)	30936.0057	0.0005	10	8	2 (3)	11	9	2 (3)	30929.1548	0.0005
22	8	14 (15)	23	7	16 (17)	30934.4255	0.0005	11	8	3 (4)	12	9	3 (4)	30928.6723	0.0005
23	8	15 (16)	24	7	17 (18)	30933.5905	0.0005	13	8	5 (6)	13	9	5 (4)	30930.0481	0.0005
24	8	16 (17)	25	7	18 (19)	30932.7246	0.0005	14	8	6 (7)	14	9	6 (5)	30929.6540	0.0005
25	8	17 (18)	26	7	19 (20)	30931.8282	0.0005	15	8	7 (8)	15	9	7 (6)	30929.2320	0.0005
26	8	18 (19)	27	7	20 (21)	30930.9010	0.0005	16	8	8 (9)	16	9	8 (7)	30928.7803	0.0005
27	8	19 (20)	28	7	21 (22)	30929.9424	0.0005	13	8	5 (6)	12	9	3 (4)	30932.3024	0.0005
28	8	20 (21)	29	7	22 (23)	30928.9528	0.0005	15	8	7 (8)	14	9	5 (6)	30931.8325	0.0005

TABLE I—*Continued*

J′	K_{-1}'	K_1'	J″	K_{-1}''	K_1''	wavenumber	error	J′	K_{-1}'	K_1'	J″	K_{-1}''	K_1''	wavenumber	error
18	8	10 (11)	17	9	8 (9)	30930.9140	0.0005	25	10	15 (16)	25	11	15 (14)	30936.8925	0.0005
19	8	11 (12)	18	9	9 (10)	30930.5505	0.0005	26	10	16 (17)	26	11	16 (15)	30936.1588	0.0005
20	8	12 (13)	19	9	10 (11)	30930.1576	0.0005	28	10	18 (19)	28	11	18 (17)	30934.6038	0.0005
21	8	13 (14)	20	9	11 (12)	30929.7369	0.0005	29	10	19 (20)	29	11	19 (18)	30933.7833	0.0005
22	8	14 (15)	21	9	12 (13)	30929.2870	0.0005	30	10	20 (21)	30	11	20 (19)	30932.9330	0.0005
23	8	15 (16)	22	9	13 (14)	30928.8078	0.0005	31	10	21 (22)	31	11	21 (20)	30932.0535	0.0005
36	10	26 (27)	37	9	28 (29)	30936.8825	0.0010	32	10	22 (23)	32	11	22 (21)	30931.1450	0.0005
37	10	27 (28)	38	9	29 (30)	30935.6357	0.0010	33	10	23 (24)	33	11	23 (22)	30930.2061	0.0005
39	10	29 (30)	40	9	31 (32)	30933.0475	0.0010	34	10	24 (25)	34	11	24 (23)	30929.2390	0.0005
40	10	30 (31)	41	9	32 (33)	30931.7058	0.0005	31	10	21 (22)	30	11	19 (20)	30937.4364	0.0005
41	10	31 (32)	42	9	33 (34)	30930.3312	0.0010	32	10	22 (23)	31	11	20 (21)	30936.7025	0.0005
42	10	32 (33)	43	9	34 (35)	30928.9253	0.0010	33	10	23 (24)	32	11	21 (22)	30935.9391	0.0005
41	10	31 (32)	41	9	33 (32)	30937.6603	0.0005	34	10	24 (25)	33	11	22 (23)	30935.1463	0.0005
42	10	32 (33)	42	9	34 (33)	30936.4319	0.0005	35	10	25 (26)	34	11	23 (24)	30934.3238	0.0005
43	10	33 (34)	43	9	35 (34)	30935.1706	0.0005	36	10	26 (27)	35	11	24 (25)	30933.4717	0.0007
44	10	35	44	9	35	30933.8769	0.0005	37	10	27 (28)	36	11	25 (26)	30932.5899	0.0005
44	10	34	44	9	36	30933.8781	0.0005	38	10	28 (29)	37	11	26 (27)	30931.6781	0.0007
45	10	36	45	9	36	30932.5501	0.0005	39	10	29 (30)	38	11	27 (28)	30930.7362	0.0005
45	10	35	45	9	37	30932.5520	0.0005	40	10	30 (31)	39	11	28 (29)	30929.7643	0.0010
46	10	37	46	9	37	30931.1896	0.0005	41	10	31 (32)	40	11	29 (30)	30928.7627	0.0005
46	10	36	46	9	38	30931.1928	0.0005	28	11	17 (18)	29	12	17 (18)	30937.4773	0.0005
47	10	38	47	9	38	30929.7959	0.0005	29	11	18 (19)	30	12	18 (19)	30936.4860	0.0005
47	10	37	47	9	39	30929.8004	0.0005	30	11	19 (20)	31	12	19 (20)	30935.4661	0.0005
48	10	38	47	9	38	30936.7658	0.0005	31	11	20 (21)	32	12	20 (21)	30934.4173	0.0005
48	10	39	47	9	39	30936.7703	0.0005	32	11	21 (22)	33	12	21 (22)	30933.3395	0.0005
49	10	40	48	9	40	30935.4895	0.0005	33	11	22 (23)	34	12	22 (23)	30932.2321	0.0005
9	9	0 (1)	10	10	0 (1)	30935.9233	0.0005	34	11	23 (24)	35	12	23 (24)	30931.0953	0.0005
10	9	1 (2)	11	10	1 (2)	30935.4693	0.0005	35	11	24 (25)	36	12	24 (25)	30929.9288	0.0005
11	9	2 (3)	12	10	2 (3)	30934.9876	0.0005	36	11	25 (26)	37	12	25 (26)	30928.7338	0.0005
12	9	3 (4)	13	10	3 (4)	30934.4777	0.0005	34	11	23 (24)	34	12	23 (22)	30937.1736	0.0005
13	9	4 (5)	14	10	4 (5)	30933.9395	0.0005	35	11	24 (25)	35	12	24 (23)	30936.1823	0.0005
14	9	5 (6)	15	10	5 (6)	30933.3722	0.0005	36	11	25 (26)	36	12	25 (24)	30935.1622	0.0005
15	9	6 (7)	16	10	6 (7)	30932.7778	0.0005	38	11	27 (28)	38	12	27 (26)	30933.0320	0.0005
16	9	7 (8)	17	10	7 (8)	30932.1541	0.0005	39	11	28 (29)	39	12	28 (27)	30931.9225	0.0005
17	9	8 (9)	18	10	8 (9)	30931.5016	0.0005	40	11	29 (30)	40	12	29 (28)	30930.7835	0.0005
18	9	9 (10)	19	10	9 (10)	30930.8212	0.0005	41	11	30 (31)	41	12	30 (29)	30929.6144	0.0005
19	9	10 (11)	20	10	10 (11)	30930.1110	0.0005	42	11	31 (32)	41	12	29 (30)	30935.7177	0.0005
20	9	11 (12)	21	10	11 (12)	30929.3737	0.0005	43	11	32 (33)	42	12	30 (31)	30934.6638	0.0005
21	9	12 (13)	22	10	12 (13)	30928.6071	0.0005	45	11	34 (35)	44	12	32 (33)	30932.4669	0.0005
11	9	2 (3)	11	10	2 (1)	30937.0673	0.0005	46	11	35 (36)	45	12	33 (34)	30931.3225	0.0005
12	9	3 (4)	12	10	3 (2)	30936.7308	0.0005	47	11	36 (37)	46	12	34 (35)	30930.1475	0.0005
13	9	4 (5)	13	10	4 (3)	30936.3659	0.0005	48	11	37 (38)	47	12	35 (36)	30928.9430	0.0010
14	9	5 (6)	14	10	5 (4)	30935.9727	0.0005	36	12	24 (25)	37	13	24 (25)	30937.4311	0.0005
15	9	6 (7)	15	10	6 (5)	30935.5513	0.0007	37	12	25 (26)	38	13	25 (26)	30936.2125	0.0005
16	9	7 (8)	16	10	7 (6)	30935.1017	0.0005	38	12	26 (27)	39	13	26 (27)	30934.9648	0.0005
17	9	8 (9)	17	10	8 (7)	30934.6233	0.0005	39	12	27 (28)	40	13	27 (28)	30933.6882	0.0005
18	9	9 (10)	18	10	9 (8)	30934.1166	0.0005	40	12	28 (29)	41	13	28 (29)	30932.3812	0.0005
20	9	11 (12)	20	10	11 (10)	30933.0174	0.0005	41	12	29 (30)	42	13	29 (30)	30931.0453	0.0005
21	9	12 (13)	21	10	12 (11)	30932.4247	0.0005	42	12	30 (31)	43	13	30 (31)	30929.6794	0.0005
22	9	13 (14)	22	10	13 (12)	30931.8032	0.0005	42	12	30 (31)	42	13	30 (29)	30937.1511	0.0005
23	9	14 (15)	23	10	14 (13)	30931.1529	0.0005	43	12	31 (32)	43	13	31 (30)	30935.9309	0.0005
25	9	16 (17)	25	10	16 (15)	30929.7643	0.0010	44	12	32 (33)	44	13	32 (31)	30934.6806	0.0005
26	9	17 (18)	26	10	17 (16)	30929.0276	0.0005	45	12	33 (34)	45	13	33 (32)	30933.4012	0.0005
18	9	9 (10)	17	10	7 (8)	30937.2377	0.0005	46	12	34 (35)	46	13	34 (33)	30932.0912	0.0005
19	9	10 (11)	18	10	8 (9)	30936.8761	0.0005	48	12	36 (37)	48	13	36 (35)	30929.3818	0.0005
21	9	12 (13)	20	10	10 (11)	30936.0678	0.0005	48	12	36 (37)	47	13	34 (35)	30937.7271	0.0005
22	9	13 (14)	21	10	11 (12)	30935.6197	0.0005	49	12	37 (38)	48	13	35 (36)	30936.5027	0.0005
23	9	14 (15)	22	10	12 (13)	30935.1435	0.0005	50	12	38 (39)	49	13	36 (37)	30935.2480	0.0005
25	9	16 (17)	24	10	14 (15)	30934.1044	0.0005	51	12	39 (40)	50	13	37 (38)	30933.9623	0.0005
26	9	17 (18)	25	10	15 (16)	30933.5414	0.0005	52	12	40 (41)	51	13	38 (39)	30932.6476	0.0005
27	9	18 (19)	26	10	16 (17)	30932.9493	0.0005	53	12	41 (42)	52	13	39 (40)	30931.3018	0.0005
29	9	20 (21)	28	10	18 (19)	30931.6766	0.0005	54	12	42 (43)	53	13	40 (41)	30929.9248	0.0005
30	9	21 (22)	29	10	19 (20)	30930.9967	0.0005	43	13	30 (31)	44	14	30 (31)	30937.7582	0.0005
31	9	22 (23)	30	10	20 (21)	30930.2866	0.0005	44	13	31 (32)	45	14	31 (32)	30936.3418	0.0005
32	9	23 (24)	31	10	21 (22)	30929.5470	0.0005	45	13	32 (33)	46	14	32 (33)	30934.8956	0.0005
33	9	24 (25)	32	10	22 (23)	30928.7782	0.0005	46	13	33 (34)	47	14	33 (34)	30933.4200	0.0005
18	10	8 (9)	19	11	8 (9)	30937.9314	0.0005	47	13	34 (35)	48	14	34 (35)	30931.9146	0.0005
19	10	9 (10)	20	11	9 (10)	30937.2245	0.0007	48	13	35 (36)	49	14	35 (36)	30930.3793	0.0005
20	10	10 (11)	21	11	10 (11)	30936.4884	0.0005	49	13	36 (37)	50	14	36 (37)	30928.8145	0.0005
21	10	11 (12)	22	11	11 (12)	30935.7248	0.0005	49	13	36 (37)	49	14	36 (35)	30937.5040	0.0005
22	10	12 (13)	23	11	12 (13)	30934.9316	0.0005	50	13	37 (38)	50	14	37 (36)	30936.0847	0.0005
23	10	13 (14)	24	11	13 (14)	30934.1102	0.0010	51	13	38 (39)	51	14	38 (37)	30934.6351	0.0005
24	10	14 (15)	25	11	14 (15)	30933.2600	0.0005	54	13	41 (42)	54	14	41 (40)	30930.1059	0.0005
25	10	15 (16)	26	11	15 (16)	30932.3812	0.0010	56	13	43 (44)	55	14	41 (42)	30936.6755	0.0005
26	10	16 (17)	27	11	16 (17)	30931.4722	0.0005	57	13	44 (45)	56	14	42 (43)	30935.2202	0.0005
27	10	17 (18)	28	11	17 (18)	30930.5352	0.0005	58	13	45 (46)	57	14	43 (44)	30933.7347	0.0005
28	10	18 (19)	29	11	18 (19)	30929.5691	0.0005	59	13	46 (47)	58	14	44 (45)	30932.2184	0.0005
29	10	19 (20)	30	11	19 (20)	30928.5738	0.0005	60	13	47 (48)	59	14	45 (46)	30930.6714	0.0005
24	10	14 (15)	24	11	14 (13)	30937.5973	0.0005								

and optical data simultaneously were, within three times the standard deviation, the same as the ones obtained from a fit of the microwave data alone (*10*). The final results of the least-squares fit for both isotopes is given in Table III. The error is equal

TABLE II

Measured Transitions of the $Si^{35}Cl^{37}Cl$ $\tilde{A}\,^1B_1(0, 6, 0) \leftarrow \tilde{X}\,^1A_1(0, 0, 0)$ Band (in Case of Unresolved K-Type Doubling the Second (K_1', K_1'') Combination Is Given in Parentheses)

J'	K_{-1}'	K_1'	J''	K_{-1}''	K_1''	wavenumber	error	J'	K_{-1}'	K_1'	J''	K_{-1}''	K_1''	wavenumber	error
16	8	8(9)	17	7	10(11)	30930.3681	0.0005	16	10	6(7)	17	11	6(7)	30930.6965	0.0007
18	8	10(11)	19	7	12(13)	30929.0586	0.0005	17	10	7(8)	18	11	7(8)	30930.0616	0.0005
10	8	2(3)	10	7	4(3)	30935.4746	0.0010	18	10	8(9)	19	11	8(9)	30929.4000	0.0005
11	8	3(4)	11	7	5(4)	30935.1724	0.0010	19	10	9(10)	20	11	9(10)	30928.7098	0.0007
12	8	4(5)	12	7	6(5)	30934.8425	0.0005	16	10	6(7)	16	11	6(5)	30933.5678	0.0005
13	8	5(6)	13	7	7(6)	30934.4844	0.0005	18	10	8(9)	18	11	8(7)	30932.6098	0.0005
14	8	6(7)	14	7	8(7)	30934.0985	0.0007	19	10	9(10)	19	11	9(8)	30932.0886	0.0005
15	8	7(8)	15	7	9(8)	30933.6845	0.0005	20	10	10(11)	20	11	10(9)	30931.5401	0.0005
16	8	8(9)	16	7	10(9)	30933.2427	0.0005	21	10	11(12)	21	11	11(10)	30930.9641	0.0005
17	8	9(10)	17	7	11(10)	30932.7718	0.0005	22	10	12(13)	22	11	12(11)	30930.3593	0.0005
18	8	10(11)	18	7	12(11)	30932.2726	0.0007	23	10	13(14)	23	11	13(12)	30929.7269	0.0005
19	8	11(12)	19	7	13(12)	30931.7448	0.0005	24	10	14(15)	24	11	14(13)	30929.0669	0.0005
8	8	0(1)	7	7	0(1)	30937.3472	0.0007	22	10	12(13)	21	11	10(11)	30934.0769	0.0005
9	8	1(2)	8	7	1(2)	30937.2685	0.0007	24	10	14(15)	23	11	12(13)	30933.1227	0.0005
10	8	2(3)	9	7	2(3)	30937.1631	0.0005	25	10	15(16)	24	11	13(14)	30932.6048	0.0005
11	8	3(4)	10	7	3(4)	30937.0299	0.0005	26	10	16(17)	25	11	14(15)	30932.0576	0.0005
12	8	4(5)	11	7	4(5)	30936.8691	0.0005	27	10	17(18)	26	11	15(16)	30931.4825	0.0005
13	8	5(6)	12	7	5(6)	30936.6801	0.0005	28	10	18(19)	27	11	16(17)	30930.8794	0.0005
14	8	6(7)	13	7	6(7)	30936.4642	0.0005	29	10	19(20)	28	11	17(18)	30930.2478	0.0005
15	8	7(8)	14	7	7(8)	30936.2192	0.0005	30	10	20(21)	29	11	18(19)	30929.5883	0.0005
16	8	8(9)	15	7	8(9)	30935.9466	0.0005	31	10	21(22)	30	11	19(20)	30928.9001	0.0005
17	8	9(10)	16	7	9(10)	30935.6456	0.0005	17	11	6(7)	18	12	6(7)	30937.8420	0.0005
18	8	10(11)	17	7	10(11)	30935.3164	0.0005	18	11	7(8)	19	12	7(8)	30937.1818	0.0005
19	8	11(12)	18	7	11(12)	30934.9583	0.0005	19	11	8(9)	20	12	8(9)	30936.4937	0.0005
20	8	12(13)	19	7	12(13)	30934.5720	0.0005	20	11	9(10)	21	12	9(10)	30935.7777	0.0005
21	8	13(14)	20	7	13(14)	30934.1571	0.0005	21	11	10(11)	22	12	10(11)	30935.0340	0.0005
22	8	14(15)	21	7	14(15)	30933.7137	0.0007	22	11	11(12)	23	12	11(12)	30934.2632	0.0005
23	8	15(16)	22	7	15(16)	30933.2405	0.0005	23	11	12(13)	24	12	12(13)	30933.4643	0.0005
24	8	16(17)	23	7	16(17)	30932.7382	0.0005	24	11	13(14)	25	12	13(14)	30932.6372	0.0005
25	8	17(18)	24	7	17(18)	30932.2070	0.0005	25	11	14(15)	26	12	14(15)	30931.7820	0.0005
26	8	18(19)	25	7	18(19)	30931.6452	0.0005	26	11	15(16)	27	12	15(16)	30930.8993	0.0005
27	8	19(20)	26	7	19(20)	30931.0546	0.0005	28	11	17(18)	29	12	17(18)	30929.0498	0.0007
28	8	20(21)	27	7	20(21)	30930.4336	0.0005	24	11	13(14)	24	12	13(12)	30936.8611	0.0005
29	8	21(22)	28	7	21(22)	30929.7823	0.0005	25	11	14(15)	25	12	14(13)	30936.1762	0.0005
30	8	22(23)	29	7	22(23)	30929.1009	0.0005	26	11	15(16)	26	12	15(14)	30935.4628	0.0005
26	9	17(18)	27	8	19(20)	30930.5627	0.0005	27	11	16(17)	27	12	16(15)	30934.7213	0.0005
27	9	18(19)	28	8	20(21)	30929.6383	0.0005	28	11	17(18)	28	12	17(16)	30933.9524	0.0005
22	9	13(14)	22	8	15(14)	30937.8637	0.0007	29	11	18(19)	29	12	18(17)	30933.1551	0.0007
23	9	14(15)	23	8	16(15)	30937.2254	0.0007	30	11	19(20)	30	12	19(18)	30932.3299	0.0005
24	9	15(16)	24	8	17(16)	30936.5581	0.0005	31	11	20(21)	31	12	20(19)	30931.4755	0.0005
25	9	16(17)	25	8	18(17)	30935.8622	0.0005	32	11	21(22)	32	12	21(20)	30930.5941	0.0007
26	9	17(18)	26	8	19(18)	30935.1368	0.0005	33	11	22(23)	33	12	22(21)	30929.6829	0.0005
27	9	18(19)	27	8	20(19)	30934.3822	0.0005	34	11	23(24)	34	12	23(22)	30928.7446	0.0005
28	9	19(20)	28	8	21(20)	30933.5986	0.0005	31	11	20(21)	30	12	18(19)	30936.7170	0.0007
29	9	20(21)	29	8	22(21)	30932.7850	0.0005	33	11	22(23)	32	12	20(21)	30935.2640	0.0005
30	9	21(22)	30	8	23(22)	30931.9416	0.0005	34	11	23(24)	33	12	21(22)	30934.4953	0.0005
31	9	22(23)	31	8	24(23)	30931.0689	0.0005	35	11	24(25)	34	12	22(23)	30933.6981	0.0005
32	9	23(24)	32	8	25(24)	30930.1649	0.0007	36	11	25(26)	35	12	23(24)	30932.8725	0.0005
33	9	24(25)	33	8	26(25)	30929.2320	0.0007	37	11	26(27)	36	12	24(25)	30932.0177	0.0005
29	9	20(21)	28	8	20(21)	30937.6987	0.0005	38	11	27(28)	37	12	25(26)	30931.1344	0.0005
30	9	21(22)	29	8	21(22)	30937.0269	0.0005	39	11	28(29)	38	12	26(27)	30930.2220	0.0005
31	9	22(23)	30	8	22(23)	30936.3251	0.0005	40	11	29(30)	39	12	27(28)	30929.2818	0.0005
32	9	23(24)	31	8	23(24)	30935.5935	0.0005	28	12	16(17)	29	13	16(17)	30937.6011	0.0005
33	9	24(25)	32	8	24(25)	30934.8317	0.0005	29	12	17(18)	30	13	17(18)	30936.6381	0.0005
34	9	25(26)	33	8	25(26)	30934.0400	0.0005	30	12	18(19)	31	13	18(19)	30935.6468	0.0005
35	9	26(27)	34	8	26(27)	30933.2177	0.0005	31	12	19(20)	32	13	19(20)	30934.6277	0.0005
36	9	27(28)	35	8	27(28)	30932.3643	0.0005	33	12	21(22)	34	13	21(22)	30932.5047	0.0005
37	9	28(29)	36	8	28(29)	30931.4802	0.0007	34	12	22(23)	35	13	22(23)	30931.4011	0.0005
38	9	29	37	8	29	30930.5642	0.0005	35	12	23(24)	36	13	23(24)	30930.2687	0.0005
38	9	30	37	8	30	30930.5652	0.0005	36	12	24(25)	37	13	24(25)	30929.1086	0.0005
39	9	30	38	8	30	30929.6177	0.0005	34	12	22(23)	34	13	22(21)	30937.3190	0.0005
39	9	31	38	8	31	30929.6195	0.0005	35	12	23(24)	35	13	23(22)	30936.3571	0.0005
40	9	31	39	8	31	30928.6390	0.0005	36	12	24(25)	36	13	24(23)	30935.3662	0.0005
40	9	32	39	8	32	30928.6412	0.0005	37	12	25(26)	37	13	25(24)	30934.3476	0.0005
33	10	23(24)	33	9	25(24)	30937.9483	0.0005	38	12	26(27)	38	13	26(25)	30933.3008	0.0005
34	10	24(25)	34	9	26(25)	30936.9951	0.0005	39	12	27(28)	39	13	27(26)	30932.2248	0.0005
35	10	25(26)	35	9	27(26)	30936.0123	0.0005	42	12	30(31)	42	13	30(29)	30928.8254	0.0005
36	10	26(27)	36	9	28(27)	30934.9993	0.0005	40	12	28(29)	39	13	26(27)	30937.8868	0.0005
37	10	27(28)	37	9	29(28)	30933.9562	0.0005	41	12	29(30)	40	13	27(28)	30936.9240	0.0005
38	10	28(29)	38	9	30(29)	30932.8829	0.0005	42	12	30(31)	41	13	28(29)	30935.9329	0.0005
39	10	29(30)	39	9	31(30)	30931.7786	0.0005	43	12	31(32)	42	13	29(30)	30934.9121	0.0005
40	10	30(31)	40	9	32(31)	30930.6440	0.0005	44	12	32(33)	43	13	30(31)	30933.8633	0.0005
41	10	31(32)	41	9	33(32)	30929.4783	0.0005	47	12	35(36)	46	13	33(34)	30930.5421	0.0005
40	10	30(31)	39	9	30(31)	30937.4352	0.0005	48	12	36(37)	47	13	34(35)	30929.3768	0.0005
41	10	31(32)	40	9	31(32)	30936.4418	0.0005	37	13	24(25)	38	14	24(25)	30937.2362	0.0005
42	10	32(33)	41	9	32(33)	30935.4178	0.0005	38	13	25(26)	39	14	25(26)	30936.0250	0.0007
43	10	33(34)	42	9	33(34)	30934.3625	0.0007	39	13	26(27)	40	14	26(27)	30934.7852	0.0005
44	10	34(35)	43	9	34(35)	30933.2766	0.0005	40	13	27(28)	41	14	27(28)	30933.5175	0.0005
45	10	35	44	9	35	30932.1575	0.0005	41	13	28(29)	42	14	28(29)	30932.2210	0.0005
45	10	36	44	9	36	30932.1584	0.0005	42	13	29(30)	43	14	29(30)	30930.8961	0.0007
46	10	36	45	9	36	30931.0064	0.0005	43	13	30(31)	44	14	30(31)	30929.5422	0.0005
47	10	37	46	9	37	30929.8248	0.0005	43	13	30(31)	43	14	30(29)	30936.9859	0.0005
47	10	38	46	9	38	30929.8273	0.0005	45	13	32(33)	45	14	32(31)	30934.5335	0.0005
43	11	32(33)	43	10	34(33)	30936.6267	0.0005	46	13	33(34)	46	14	33(32)	30933.2637	0.0005
44	11	33(34)	44	10	35(34)	30935.3837	0.0005	47	13	34(35)	47	14	34(33)	30931.9664	0.0005
46	11	35(36)	46	10	37(36)	30932.8059	0.0005	48	13	35(36)	48	14	35(34)	30930.6394	0.0005
47	11	36(37)	47	10	38(37)	30931.4696	0.0005	49	13	36(37)	49	14	36(35)	30929.2837	0.0005
48	11	37(38)	48	10	39(38)	30930.1028	0.0005	49	13	36(37)	48	14	34(35)	30937.5767	0.0005
49	11	38(39)	49	10	40(39)	30928.7055	0.0010	50	13	37(38)	49	14	35(36)	30936.3626	0.0005
10	10	0(1)	11	11	0(1)	30933.9255	0.0005	51	13	38(39)	50	14	36(37)	30935.1195	0.0005
11	10	1(2)	12	11	1(2)	30933.4563	0.0005	52	13	39(40)	51	14	37(38)	30933.8472	0.0005
12	10	2(3)	13	11	2(3)	30932.9596	0.0005	53	13	40(41)	52	14	38(39)	30932.5456	0.0005
13	10	3(4)	14	11	3(4)	30932.4350	0.0007	54	13	41(42)	53	14	39(40)	30931.2149	0.0005
14	10	4(5)	15	11	4(5)	30931.8833	0.0005	55	13	42(43)	54	14	40(41)	30929.8543	0.0005
15	10	5(6)	16	11	5(6)	30931.3039	0.0005								

TABLE III

Results of the Least Squares Fit of Both Microwave Data (*10*) and Optical Data to an Asymmetric Rotor Model (*20*) for $Si^{35}Cl_2$ and $Si^{35}Cl^{37}Cl$ (the Error is Equal to Three Times the Standard Deviation)

Constants	$Si^{35}Cl_2$	$Si^{35}Cl^{37}Cl$	Units
A"	14781.088 ± 0.016	14667.339 ± 0.032	MHz
B"	2822.3967 ± 0.0040	2745.4976 ± 0.0049	MHz
C"	2366.4836 ± 0.0040	2309.3650 ± 0.0045	MHz
Δ_J" $\cdot 10^3$	1.362 ± 0.021	1.280 ± 0.024	MHz
Δ_{JK}" $\cdot 10^3$	-14.905 ± 0.096	-14.22 ± 0.20	MHz
Δ_K" $\cdot 10^3$	139.4 ± 1.8	136.1 ± 1.9	MHz
δ_J" $\cdot 10^3$	0.3282 ± 0.0018	0.3118 ± 0.0021	MHz
δ_K" $\cdot 10^3$	3.96 ± 0.14	3.32 ± 0.26	MHz
H_K" $\cdot 10^6$	0.0	0.0	MHz
ν_{60}	30912.2876 ± 0.0060	30904.0296 ± 0.0060	cm^{-1}
A'	27260.55 ± 1.16	26998.24 ± 2.14	MHz
B'	2284.95 ± 1.74	2223.71 ± 2.94	MHz
C'	2059.55 ± 1.87	2006.69 ± 3.11	MHz
(B'+C')/2	2172.247 ± 0.088	2115.196 ± 0.131	MHz
Δ_J' $\cdot 10^3$	1.172 ± 0.032	1.094 ± 0.039	MHz
Δ_{JK}' $\cdot 10^3$	-65.88 ± 0.75	-62.19 ± 0.78	MHz
Δ_K' $\cdot 10^3$	2584.4 ± 12.9	2507.3 ± 20.4	MHz
δ_J' $\cdot 10^3$	0.0	0.0	MHz
δ_K' $\cdot 10^3$	0.0	0.0	MHz
H_K' $\cdot 10^6$	446.7 ± 38.5	456.3 ± 58.4	MHz
I_a'	18.5388 ± 0.0008	18.7189 ± 0.0015	amu·Å^2
I_b'	221.17 ± 0.17	227.26 ± 0.30	amu·Å^2
I_c'	245.38 ± 0.23	251.84 ± 0.39	amu·Å^2
Δ	5.67 ± 0.29	5.86 ± 0.50	amu·Å^2
stand. dev.	12.0	11.5	MHz

to three times the standard deviation. For the values of B' and C' a relatively large error is found; this is due to the fact that the K-type doubling in the $\tilde{A}^1B_1(0, 6, 0)$ state could not be resolved, which means that $(B' - C')/2$ could not be accurately determined. The more accurately determined value for $(B' + C')/2$ is therefore given as well. From the distortion-free rotational constants in the $\tilde{A}^1B_1(0, 6, 0)$ state (*21*), the moments of inertia I'_a, I'_b, and I'_c, as well as the inertia defect $\Delta = I'_c - I'_b - I'_a$, are determined.

In the upper half of Fig. 2 a part of the observed LIF spectrum ($\Delta\nu_{FWHM} \approx 30$ MHz) is shown. All strong lines are identified and it is seen that the spectrum is quite complex. This part of the spectrum is chosen for representation because at least four lines belonging to the same branch ($Si^{35}Cl_2$ $^rR_5$ branch) can be seen. The underlined lines belong to the $Si^{35}Cl^{37}Cl$ isotope. The $Si^{35}Cl_2$ $\tilde{X}^1A_1(0, 0, 0)$ $J'' = 20$, $K''_a = 6$ level, probed via the $^rQ_6(20)$ transition as shown in Fig. 2, is calculated to have a relative population of only 10^{-4}, if a rotational and vibrational temperature of 400 K is assumed. From the absolute intensity of the observed LIF signal, the known fluorescence detection efficiency, and the known excitation rate (from the Lamb dip ex-

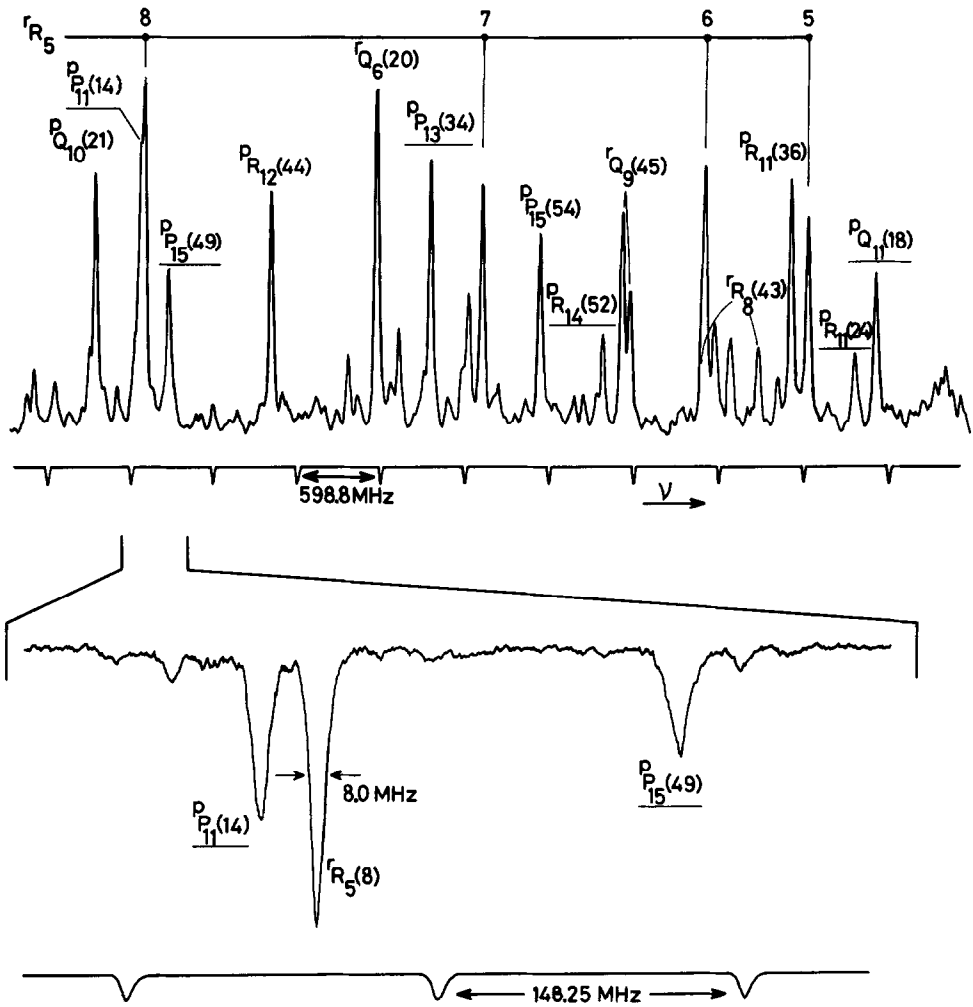

FIG. 2. Upper half: part of the observed $SiCl_2$ ($\tilde{A} \leftarrow \tilde{X}$) LIF spectrum around 323 nm. The identified rotational transitions are indicated. Underlined transitions belong to the less abundant $Si^{35}Cl^{37}Cl$ isotope. Lower half: high-resolution Lamb dip spectrum of the region around the $Si^{35}Cl_2$ $^rR_5(8)$ line. The observed linewidth of 8 MHz is most probably due to unresolved hyperfine structure.

periment), it is concluded that at least 10% of the beam consists of $SiCl_2$ radicals. In Fig. 2 it is demonstrated that even for $K''_a = 9$ the K-type doubling can be resolved when J'' is as high as 45 ($Si^{35}Cl_2$; $^rQ_9(45)$). The expected intensity alternation in the resolved K-doublets of 5:3 due to the spin $I = \frac{3}{2}$ of the chlorine nucleus is seen. As there are 10 symmetric spin wave functions and only 6 antisymmetric ones, strongest lines are expected from ground state levels with a wavefunction that is antisymmetric with respect to $C_2(b)$ rotation. This implies that strongest lines are expected from levels with $K''_a + K''_c$ odd. The intensity alternation provides an additional check on the J, K assignment as well as on the isotope assignment.

In the lower half of Fig. 2 a part of the spectrum is shown with an improved spectral resolution, using the aforementioned Lamb dip technique. The observed linewidth of $\Delta\nu_{FWHM} \approx 8$ MHz is somewhat larger than expected from the finite lifetime of the excited state ($\tau = 77 \pm 3$ ns for $\nu_2' = 7$ (*8*), which implies $\Delta\nu_\tau \approx 2$ MHz). Other broadening effects are known to be less than 1.5 MHz (*17*). The 8-MHz linewidth we observe might therefore be due to unresolved hyperfine structure in both electronic states.

Although the line positions could be fitted very well and did not show the effect of any perturbation, the intensity of the different branches did not follow the expectations. Especially the ^pR branches were too strong (by a factor of 1.5–2.5) relative to the ^pP branches, whereas the ^pQ branches were too weak (by a factor of about 2), especially for higher J''. For the $\Delta K = +1$ branches the ^rQ and ^rP branches are about 50% too strong, when compared with the ^rR branches. At the moment we do not have a clear explanation for these intensity anomalies. Similar observations in the infrared spectra of NO_2 (*22*) are explained by a Coriolis mixing of other vibrational states from which much stronger transitions are possible. Then only a slight energy perturbation but a large intensity perturbation is expected. In the spectra of diatomic molecules intensity anomalies between P and R lines are often explained by the rotational dependence of the transition dipole moment (*23*), the so-called Herman–Wallis effect (*24*).

4. DISCUSSION

From the constants given in Table III, the distortion-free rotational constants in both electronic states are calculated (*21*). For $Si^{35}Cl_2$ and $Si^{35}Cl^{37}Cl$ the geometrical structure in the $\tilde{X}^1A_1(0, 0, 0)$ as well as in the $\tilde{A}^1B_1(0, 6, 0)$ is then determined and given in Table IV. Obviously, only two rotational constants are required to determine the Si–Cl bond length (R) and the ClSiCl bond angle (Θ). Due to the planarity defect slightly different results are found using the set (A, B) and the set (A, C). The difference between both results indicates the uncertainty in the values of R and Θ thus obtained. The large opening up in ClSiCl bond angle in going from $\tilde{X}$ to $\tilde{A}$, as well as the concurrent slight decrease in Si–Cl bond distance, is in qualitative agreement with theoretical calculations (*11, 12*).

We find the band origin ν_{60} for the $\tilde{A}^1B_1(0, 6, 0) \leftarrow \tilde{X}^1A_1(0, 0, 0)$ transition in $Si^{35}Cl_2$ to be almost 10 cm^{-1} higher than the value reported by Suzuki *et al.* (*8*). This is not surprising because the latter authors could not resolve any rotational structure and determined the center of the at least 20 cm^{-1} broad vibrational bands. This also strongly suggests that the band origin ν_{00} they found (*8*) has to be increased by almost 10 cm^{-1}. In this way a value of $\nu_{00} = (30\,013.4 \pm 1.0)$ cm^{-1} is obtained for the $Si^{35}Cl_2$ ($\tilde{A}^1B_1(0, 0, 0) \leftarrow \tilde{X}^1A_1(0, 0, 0)$) transition. The isotope shift determined by Suzuki *et al.* (*8*), important for the vibrational state numbering, is still correct because only relative band positions are important for this. We find a very accurate value of (8.2580 ± 0.0021) cm^{-1} for this shift, in agreement with their result (*8*).

To check the vibrational assignment as given by Suzuki *et al.* (*8*) transitions to different ν_2' levels have to be included. It is possible, however, to determine the ν_2' quantum number from the absolute value of the observed isotope shift. For this the force constants need to be known, and a negligible electronic isotope shift has to be assumed. The ν_2' quantum number can also be determined from the observed value

TABLE IV

Calculated SiCl Bond Length (in Å) and ClSiCl Bond Angle (in Degrees) for the $\tilde{X}\,^1A_1(0, 0, 0)$ and $\tilde{A}\,^1B_1(0, 6, 0)$ states of $Si^{35}Cl_2$ and $Si^{35}Cl^{37}Cl$

		$Si^{35}Cl_2$		$Si^{35}Cl^{37}Cl$	
		$R_{Si\text{-}Cl}$	$\Theta_{Cl\text{-}Si\text{-}Cl}$	$R_{Si\text{-}Cl}$	$\Theta_{Cl\text{-}Si\text{-}Cl}$
$X\,^1A_1(0,0,0)$	A",B"	2.067	101.47	2.066	101.47
	A",C"	2.068	101.52	2.067	101.52
$\tilde{A}\,^1B_1(0,6,0)$	A',B'	2.022	123.12	2.022	123.06
	A',C'	2.042	123.72	2.042	123.67

of the inertia defect. The inertia defect Δ is known to consist out of different contributions, and can in general be written as a sum of vibrational (Δ_{vib}), centrifugal (Δ_{cent}) and electronic (Δ_{elec}) contributions (*25*). The main contribution comes from Δ_{vib} (*15*), which can be expressed as

$$\Delta_{vib} = \Delta_1(v_1 + \tfrac{1}{2}) + \Delta_2(v_2 + \tfrac{1}{2}) + \Delta_3(v_3 + \tfrac{1}{2}). \quad (1)$$

Both Δ_1 and Δ_3 are small, and as they are also of opposite sign the actual value of Δ will be almost completely determined by Δ_2, which can be written as (*25*)

$$\Delta_2\,[\text{amu}\cdot\text{Å}^2] = \frac{134.86}{\nu_2\,[\text{cm}^{-1}]}\cdot\frac{\nu_3^2}{(\nu_3^2 - \nu_2^2)}\cdot|\zeta_{23}^{(c)}|^2. \quad (2)$$

Although ν_3 has not been experimentally determined yet, its value is predicted from ab initio calculations to be much larger than ν_2 (683 cm^{-1} (*12*) versus 149.9 cm^{-1} (*8*)). The Coriolis term $|\zeta_{23}^{(c)}|^2$ is expected to have a value close to its maximum value of 1 (*15*). This yields $\Delta_2 \approx 0.90$ amu · Å^2, which confirms the ν_2' numbering.

Although ab initio calculations (*11, 12*) predict that the $A \leftarrow X$ electronic transition is a *c*-type transition, the spectrum could be fitted assuming *c*-type as well as *b*-type selection rules. Only when the effects of the *K*-type doubling in the upper state are seen can one unambiguously determine the direction of the transition dipole moment. Transitions to low K_a' values are needed for this, but these lie in a spectral region that is too crowded (even at our resolution) to be completely resolved. A microwave–optical double-resonance experiment has been tried to solve this problem, but without success yet.

ACKNOWLEDGMENTS

We thank Professor A. Dymanus and Jean Schleipen for helpful and stimulating discussions. We gratefully acknowledge Dr. M. Tanimoto who sent us the observed microwave data prior to publication. Without these data the analysis of the UV spectrum would have been much more complicated. This work has been supported by the Stichting voor Fundamenteel Onderzoek der Materie (FOM) and has been made possible by financial support from the Nederlandse Organisatie voor Wetenschappelijk Onderzoek (NWO).

RECEIVED: March 16, 1989

REFERENCES

1. R. K. ASUNDI, M. KARIM, AND R. SAMUEL, *Proc. Phys. Soc. London* **50,** 581–598 (1938).
2. R. CORNET AND I. DUBOIS, *J. Phys. B* **10,** L69–71 (1977).
3. K. WIELAND AND M. HEISE, *Angew. Chem.* **63,** 438 (1951).
4. D. E. MILLIGAN AND M. E. JACOX, *J. Chem. Phys.* **49,** 1938–1942 (1968).
5. B. P. RUZSICSKA, A. JODHAN, I. SAFARIK, O. P. STRAUSZ, AND T. N. BELL, *Chem. Phys. Lett.* **113,** 67–70 (1985).
6. N. WASHIDA, Y. MATSUMI, T. HAYASHI, T. IBUKI, A. HIRAYA, AND K. SHOBATAKE, *J. Chem. Phys.* **83,** 2769–2774 (1985).
7. D. SAMEITH, J. P. MONCH, H.-J. TILLER, AND K. SCHADE, *Chem. Phys. Lett.* **128,** 483–488 (1986).
8. M. SUZUKI, N. WASHIDA, AND G. INOUE, *Chem. Phys. Lett.* **131,** 24–30 (1986).
9. R. C. SAUSA AND A. M. RONN, *Chem. Phys.* **96,** 183–189 (1985).
10. M. TANIMOTO, private communication; N. M. TANIMOTO, H. TAKEO, AND C. MATSUMURA, "Proceedings of the 49th Spring Conf. of the Chem. Soc. of Japan," Vol. 1, p. 6, 1984.
11. R. K. GOSAVI AND O. P. STRAUSZ, *Chem. Phys. Lett.* **123,** 65–68 (1986).
12. T.-K. HA, M. T. NGUYEN, M. C. KERINS, AND J. FITZPATRICK, *Chem. Phys.* **103,** 243–251 (1986).
13. W. UBACHS, J. J. TER MEULEN, AND A. DYMANUS, *Canad. J. Phys.* **62,** 1374–1391 (1984).
14. G. MEIJER, B. JANSEN, J. J. TER MEULEN, AND A. DYMANUS, *Chem. Phys. Lett.* **136,** 519–526 (1987).
15. R. N. DIXON AND M. HALLE, *J. Mol. Spectrosc.* **36,** 192–203 (1970).
16. W. A. MAJEWSKI, *Opt. Commun.* **45,** 201–205 (1983).
17. G. MEIJER, W. UBACHS, J. J. TER MEULEN, AND A. DYMANUS, *Chem. Phys. Lett.* **139,** 603–611 (1987).
18. S. GERSTENKORN AND P. LUC, "Atlas du spectroscopie d'absorption de la molecule d'iode," C.N.R.S., Paris, 1978; *Rev. Phys. Appl.* **14,** 791–794 (1979).
19. G. HERZBERG, "Molecular Spectra and Molecular Structure," Vols. 2 and 3, Van Nostrand, Princeton, 1966.
20. J. K. G. WATSON, *J. Chem. Phys.* **46,** 1935–1949 (1967); *J. Chem. Phys.* **48,** 4517–4524 (1968).
21. W. GORDY AND R. L. COOK, "Microwave Molecular Spectra," Interscience, New York, 1970.
22. A. CABANA, M. LAURIN, W. J. LAFFERTY, AND R. L. SAMS, *Canad. J. Phys.* **53,** 1902–1926 (1975).
23. J. B. BURKHOLDER, P. D. HAMMER, C. J. HOWARD, A. G. MAKI, G. THOMPSON, AND C. CHACKERIAN, JR., *J. Mol. Spectrosc.* **124,** 139–161 (1987).
24. R. H. TIPPING AND R. M. HERMAN, *J. Mol. Spectrosc.* **36,** 404–413 (1970).
25. T. OKA AND Y. MORINO, *J. Mol. Spectrosc.* **6,** 472–482 (1961).